Modeling Carbon Nitride Materials

A Major Qualifying Project (MQP) Report
Submitted to the Faculty of
WORCESTER POLYTECHNIC INSTITUTE
in partial fulfillment of the requirements
for the Degree of Bachelor of Science in

Chemical Engineering

By:

Naomasa Tanaka

Project Advisor:

Professor Aaron Deskins

Date: April 25 2023

Abstract

In this project, density functional theory (DFT) was used to model planar and corrugated structures of graphitic carbon nitride (g-C_3N_4) doped with different non-metal elements (B,O,S,P) to assess their potential as a photocatalyst. Cobalt adsorption onto corrugated boron doped g-C_3N_4 was also modeled. Properties such as the density of states and band gap were considered for all structures which we modeled. The strength of CO_2 adsorption onto the cobalt loaded boron doped g-C_3N_4 was also calculated. Results from the density of states and band gap showed that doping planar g-C_3N_4 with sulfur and boron narrows the band gap and allows for a wider range of light absorption. It was also found that doping, as well as cobalt loading, introduces defect states into the band gap of g-C_3N_4 which could be beneficial for photocatalysis as reaction sites. CO_2 adsorption onto the corrugated cobalt loaded boron doped g-C_3N_4 was found to be weaker than that of g-C_3N_4 and cobalt loaded g-C_3N_4, indicating some synergy between cobalt and boron. Further work is needed to fully assess the potential of these materials as photocatalysts.

Contents

List of Figures

List of Tables

Executive Summary

Graphitic carbon nitrides are a class of sheet-like materials that have properties suited for driving the carbon dioxide reduction reaction using light. Our project goal was to model and predict the photocatalytic properties of different graphitic carbon nitride (g-C_3N_4) materials using density functional theory (DFT) calculations using the Perdew-Burke-Ernzerhof (PBE) exchange-correlation functional. We modeled substitutional doping with non-metal elements (B,O,S,P) along with cobalt loading and corrugation of the sheets. The most stable geometries for these structures were evaluated and we compared formation energies, bond lengths, and dopant charges. Boron was found to be stable when substituting carbon atoms. Sulfur and oxygen prefer substituting the aromatic nitrogen atoms facing the heptazine pocket. Phosphorus was most stable when binding to nitrogen atoms while nesting inside of the pocket. Cobalt loading onto boron doped graphitic carbon nitride was also modeled. Our results showed that the cobalt atom loaded onto boron doped graphitic carbon nitride is more stable than over pristine graphitic carbon nitride. The stability of planar and corrugated models for graphitic carbon nitride doped with boron, oxygen, and sulfur were also compared. Graphitic carbon nitride was found to have a more stable corrugated structure for its pristine and boron doped structures.

It was found that the band gap of graphitic carbon nitride narrows with boron doping, sulfur doping, and cobalt loading. Oxygen doping, and corrugation were found to enlarge the band gap. The shortening of the band gap from boron/sulfur doping and cobalt loading allows for graphitic carbon nitride to absorb a wider range of light, improving its performance as a photocatalyst. The density of states plots for each structure revealed that doping with non-metal elements and cobalt loading introduces new defect states into the band gap. These states could reduce the minimum energy required for electrons to excite into the conductance band, enhancing the carbon dioxide reduction reaction. These calculations were rerun with the more accurate Heyd-Scuseria-Ernzerhof 2006 (HSE06) functional for pristine, boron doped, and boron doped, cobalt loaded graphitic carbon nitrides. This revealed that

the PBE functional underestimates the band gap of graphitic carbon nitride materials by 1.00 eV, but is accurate in predicting the existence of defect states within the band gap.

Finally, to assess the reactivity of carbon dioxide in our structures, carbon dioxide adsorption was modeled onto pristine, boron doped, and cobalt loaded boron doped variants of corrugated graphitic carbon nitrides. The strength of adsorption of these models was shown to be weaker than that of previous literature values produced by DFT calculations. Our models also show that boron doping and cobalt doping both weaken carbon dioxide adsorption on graphitic carbon nitride.

Overall, this endeavor found that boron doping, sulfur doping, and cobalt loading can provide an advantage for carbon dioxide reduction of carbon nitride materials by narrowing and introducing defect states into their band gap. For cobalt loaded and boron doped systems, this comes with the drawback of weaker carbon dioxide adsorption onto its surface. Future work should evaluate the effect of cobalt loading on other doped systems explored in this work, and further analyze the potential of the systems we modeled in this project by estimating other properties which could prove useful for carbon dioxide reduction such as its band structure and electron-hole recombination rate. A more long-term project could expand upon the variety of dopant types considered in this project, which would prove useful for understanding the mechanism of carbon dioxide on doped graphitic carbon nitride.

1 Introduction

From the start of the 20th century to now, the temperature of the earths' climate was estimated to have increased by an average of 1.15 C°due to the release of greenhouse gases from human activities.[1] This phenomena, also called global warming, is expected to intensify as more gases are released into the atmosphere. To avoid a climate catastrophe as outlined in the World Meteorological Organization report, there is a need to decrease the amount of greenhouse gases present on earth. One prominent greenhouse gas released by humans is carbon dioxide(CO_2) which is produced as a byproduct of combustion used to drive several industrial processes, including transportation, energy and manufacturing. Several efforts have been made to decrease carbon dioxide levels in the atmosphere through the development of technologies such as CO_2 reduction and carbon capture. Photo-catalytic carbon dioxide reduction is one such technique which has gained attention in recent years. This process converts CO_2 into useful products such as methanol through a reaction driven by light. Due to the reduction process being driven by light, there is potential for the process to be renewable and thus reduce the level of CO_2 in the atmosphere without the consumption of fossil fuels.[2]

Currently, the process of photo-catalytic CO_2 reduction faces several limitations which hinder its performance. The first of these being the stability of the carbon dioxide molecule itself. Converting CO_2 into valuable products requires that the carbon-oxygen double bond of the CO_2 molecule being broken, which requires a potential of 1.9 V.[3] There is also the challenge of CO_2 reduction reactions having to compete against the more energy efficient hydrogen evolution reaction(HER). The reduction process is also known to produce multiple products such as methane, methanol, and acetic acid.[3] To ensure that the reduction reaction is profitable, the reduction reaction must selectively produce high value products such as methanol and syngas.[4]

Graphitic carbon nitride (g-C_3N_4) is a graphite-like material with an interchanging ni-

trogen/carbon pattern, first claimed to be synthesised by Berzelius and Liebig.[5] After its discovery, the potential of carbon nitride as a photo-catalyst was evaluated by Wang et al as a suitable candidate for water splitting owing to its band gap of 2.7 eV. His team found that this band gap encompassed both the oxidation level and reduction level required to drive the process.[6] A later study by Dong and Zhang reported that carbon nitride structures can also act as a photocatalyst for carbon dioxide reduction in the visible light range.[7] Some drawbacks of g-C_3N_4 have been found for this material however, such as a high electron-hole recombination rate and weak light absorption of light above 460 nm.[8–10] There is also the need to increase reactivity of individual reaction sites.

Current efforts in improving the catalytic properties of C_3N_4 have introduced several methods to circumvent its limitations. One such method introduces defects into the repeating structure of graphitic carbon nitride through substitutional doping. This process would ideally narrow the band gap of a material, thus increasing the range of light it can absorb. Previous density functional theory (DFT) calculations combined with experimental results from various authors predict that doping of non-metal atoms such as oxygen,[11] sulfur,[12] boron[13] into g-C_3N_4 does indeed narrow its band gap. Another study which combined experimental results with DFT by Ranjbakhsh et al.,[14] showed that phosphorus doping would enlarge the band gap of g-C_3N_4 and in turn decrease the electron-hole recombination rate.

Loading of single-atom transition metals over the carbon nitride surface also remains a widely studied method of enhancing the catalytic properties of g-C_3N_4. DFT calculations from authors such as Ao et al and Homlamai et al report an increase in photo-catalytic activity from transition metal loaded C_3N_4 in general, with Fe and Co proving to be most promising.[15,16] In this study, we evaluated the properties of doped g-C_3N_4 in both planar and corrugated forms using DFT calculations. More specifically, the focus was on g-C_3N_4 sheets doped with non-metal atoms and loaded with single Co atoms. The stability of each defect was evaluated from its formation energy, and the electronic properties of the boron

doped g-C_3N_4 was calculated through its density of states. Results from these calculations assess the potential of doped, metal-loaded g-C_3N_4 as photo-catalysts, and provide insight into the mechanisms at which CO_2 reduction could occur on its surface.

2 Methodology

2.1 Computational Details

Density functional theory calculations were conducted using the Vienna Ab initio Simulation Package (VASP).[17–20] A plane wave basis set was used to represent valence electrons, with a cutoff energy set to 450eV. Core electrons were represented by projector augmented wave (PAW) potentials.[21,22] Geometry optimization was performed using the generalized gradient approximation (GGA) method with the Perdew-Burke-Ernzerhof (PBE) exchange correlation functional,[23,24] with the HSE06 functional[25] reserved for some density of states calculations. A Van der Waals correction with Becke-Johnson damping (D-3)[26,27] was used to approximate dispersion forces. A Gaussian electronic smearing scheme was used with a smearing width of 0.1 eV for geometry optimization and 0.03 eV for electronic property calculations. A base 2x2x1 supercell containing 24 carbon atoms and 32 nitrogen atoms (see Figure1 was used with a 15 Å vacuum space set in the z-axis to ensure proper separation between carbon nitride sheets. The size of the supercell allows for the modelling of cobalt sites both with and without an adjacent dopant and allows introduction of corrugation into g-C_3N_4. For geometry optimization of pristine g-C_3N_4, doped g-C_3N_4, and cobalt-loaded g-C_3N_4, a Monkhorst-Pack k-point mesh of 2x2x1 was used for sampling of the Brillouin zone.[28] The electronic properties of each structure was calculated from a Monkhorst-Pack k-point mesh of 5x5x1 when using the PBE functional. A 2x2x1 gamma-centered mesh was applied when calculating the band gap and density of states using the HSE06 functional.

2.2 Stability of Doped g-C_3N_4

The four elements oxygen, sulfur, boron, and phosphorus were chosen as potential dopants for g-C_3N_4 based on results from previous authors.[11–14] For each dopant, a total of six potential doping sites were identified for this study, as shown in Figure 1. A notation system to locate each dopant cite was established, where N1, N2, and N3 are sites where the dopant atom replaces a nitrogen atom, and C1 and C2 are sites where the dopant atom replaces a carbon atom. Due the symmetrical structure of graphitic carbon nitride, the ringed N atoms facing the heptazine pocket can be categorized as the same doping site N2. Similarly the N atom acting as the bridge between one carbon nitride flake to the other was designated as N3, and the N atom in the center of the ringed structure was designated as N1. A distinction was also made between the C atoms in the carbon nitride structure which are close to the center N atom, and can be categorized as C1 and C2 respectively. A configuration where the dopant atom adsorbs into the interstitial site was also considered as a potential site named I1. This decision was motivated by DFT results from Gorai et al,[29] which concluded that this site is preferred over substitutional sites for phosphorus doping on g-C_3N_4.

The stability of a doped structure was assessed through its formation energy. The formation energy of a structure is calculated from the difference in energy of a structure and the molecules which form it. In the case of carbon nitride doping, this becomes:

$E_{form} = E_{DopedC_3N_4} - E_{C_3N_4} - E_{Dopant} + E_R$,

where $E_{DopedC_3N_4}$ is the energy of the doped system, $E_{C_3N_4}$ is the energy of pristine g-C3N4, E_{Dopant} is the energy of the dopant in elemental form, and E_R is the energy of the atom (C or N) replaced by the dopant. The energies and elemental forms of the atoms used for E_{Dopant} are shown in table 1. A distinction between g-C_3N_4 formed in carbon rich environments and nitrogen rich environments was also made in calculating formation energies, similar to Wei et al.[30] The energy of the atom replaced (E_R) in nitrogen rich environments was calculated from these equations:

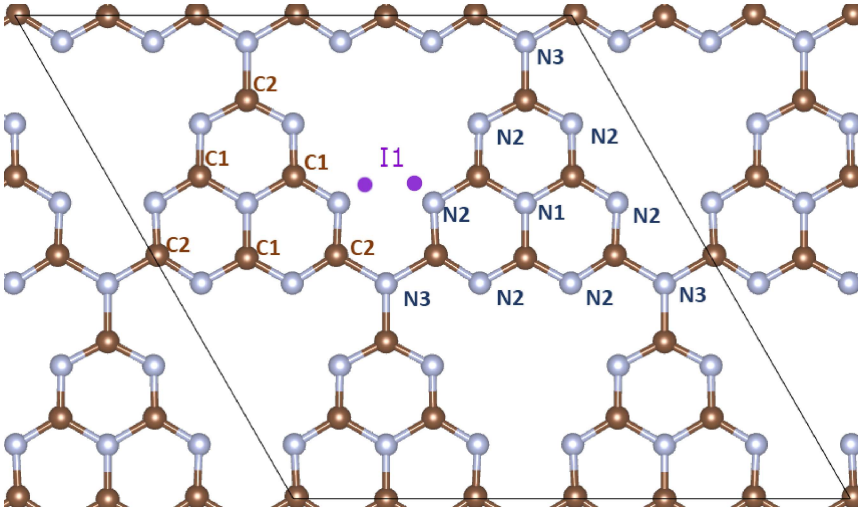

Figure 1: Dopant sites considered in this study. Shown is the (2x2) cell used to simulate g-C_3N_4. The carbon atoms(brown) close to the center of the g-C_3N_4 flake are designated as C1, with carbons farther from the center designated as C2. Nitrogen atoms(blue) located at the center of the g-C_3N_4 flake are labeled as N1 with atoms second closest to the center labeled as N2 as so on. I1 shows an interstitial site where an element could adsorb into the heptazine pocket instead of substituting a carbon or nitrogen atom.

$E_N = E_{N_2}/2$

$E_C = (E_{C_3N_4} - 2E_N)/3,$

where E_{N_2} is the energy of an isolated nitrogen gas molecule, $E_{C_3N_4}$ is the energy of a single unit of graphitic carbon nitride, E_N is the energy of the replaced nitrogen atom and E_C is the energy of the replaced carbon atom. Similarly, for carbon rich environments the energy of each replaced atom was calculated through the equations:

$E_C = E_{graphite}/4$

$E_N = (E_{C_3N_4} - 3/2E_C)/4,$

where $E_{graphite}$ is the energy of a graphite sheet with four atoms, $E_{C_3N_4}$ is the energy of graphitic carbon nitride, E_N is the energy of the replaced N atom and E_C is the energy of the replaced C atom. For the formation energy of an interstitial adsorption site, the following equation was used: $E_{form} = E_{DopedC_3N_4} - E_{C_3N_4} - E_{Dopant}$.

The energy of the replaced atom E_R is not considered here as there are no substituted atoms in this structure.

Table 1: Table of bulk species used to calculate the E_{Dopant} term in the formation energy equation.

Dopant	Chemical Formula and Phase	Total Energy(eV)	E_{Dopant} (eV)
Boron	Rhombohedral Boron (B_{36})	-249	-6.91
Sulfur	Octasulfur (S_8)	-33.5	-4.19
Oxygen	Oxygen Gas (O_2)	-9.86	-4.93
Phosphorus	Tetraphosphorus (P_4)	-21.2	-5.30

2.3 Cobalt Absorption on Doped g-C_3N_4

Several sites for Co absorption over doped carbon nitride were considered in the heptazine pockets as shown in Figure2. The adsorption energy of the Co atom was then calculated using this equation:

$E_{Ads} = E_{Co+DopedC_3N_4} - E_{DopedC_3N_4} - E_M$.

Here $E_{Co+DopedC_3N_4}$ is the energy of the Co-loaded doped graphitic carbon nitride, $E_{DopedC_3N_4}$ is the energy of the doped graphitic carbon nitride and E_M is the energy of a Co atom.

We initially assessed the effect of multiciplity by calculating the energies of a cobalt atom with different NUPDOWN settings (between zero and five). The NUPDOWN setting which returned the lowest energy was then used for all subsequent calculations which include cobalt atoms. We found that using the default value of NUPDOWN (no multiplicity specified) gave the lowest energies. We therefore used the default NUPDOWN values for our calculations.

2.4 Adsorption of CO_2 on g-C_3N_4 Surfaces

Zhu et al. reported that the adsorption energy of CO_2 on C_3N_4 is dependent on the adsorption site, as well as the orientation at which the molecule is facing the g-C_3N_4 surface.[31] To quantify the stability of CO_2 adsorption on cobalt loaded boron doped g-C_3N_4, an adsorption energy was calculated for CO_2 adsorption on top of all dopant sites in both vertical and horizontal orientations. The equation used to calculate the adsorption energy of CO_2 on a surface was:

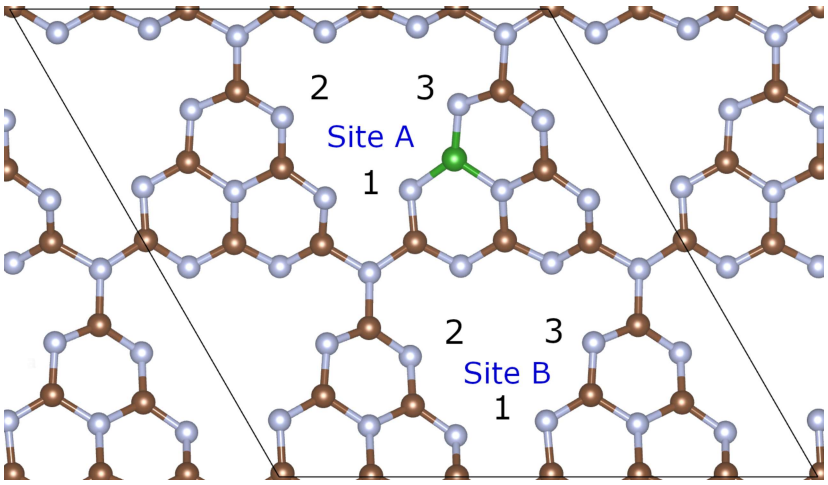

Figure 2: Possible metal adsorption sites on the g-C_3N_4 surface with a dopant atom (green sphere) present. A sites are near the dopant while B sites are far from the dopant.

$E_{Ads-CO_2} = E_{CO_2+Surface} - E_{Surface} - E_{CO_2}$.

Here E_{Ads-CO_2} is the adsorption energy, $E_{CO_2+Surface}$ is the energy of the final structure with CO_2 adsorbed on the surface, $E_{Surface}$ is the energy of the original surface, and E_{CO_2} is the energy of a lone CO_2 molecule.

3 Results and Discussion

3.1 Pristine g-C_3N_4

Before modeling the doped structures of g-C_3N_4, geometry optimization was run on a 2x2x1 cell of pristine g-C_3N_4 with a vacuum space of 15 Å in the vertical direction. Figure 3 shows the optimized structure of this pristine planar g-C_3N_4. The lattice parameter for this structure was 14.26Å (7.13 Å for a 1x1 unit cell) which agrees well with experimental values and previous DFT calculations.[6,32,33] These results validate our modeling approach.

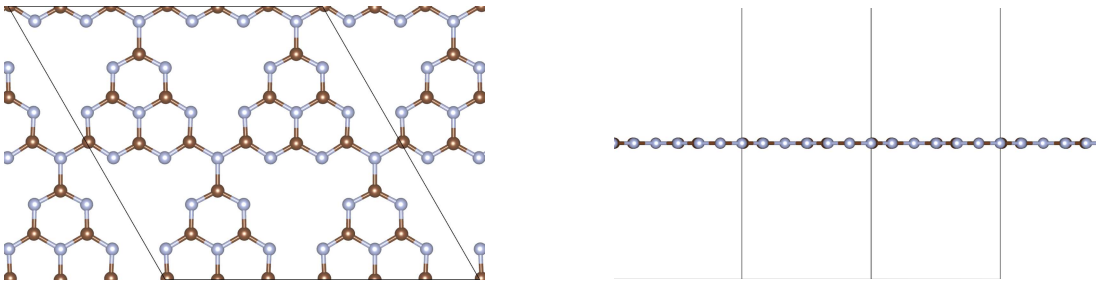

(a) (b)

Figure 3: DFT results of pristine flat g-C_3N_4 from two views: (a)Top view (b)Side view

The bond distances of pristine g-C_3N_4 are shown in Table 2. The distances between each atom agree with previous DFT results from Wei, who reported bond lengths of 1.39 Å, 1.34 Å, 1.34 Å, and 1.48 Å for N1–C1, C1–N2, N2–C2, and C2–N3, respectively.[30] To corrugate the flat g-C_3N_4 structure, a perturbation was introduced into the plane by shifting an atom in the z-direction before optimization. The final structure of corrugated g-C_3N_4 is shown in Figure 4. Corrugating the flat g-C_3N_4 reduced its overall energy by 2.7 eV as well as its lattice length to 13.83 Å. These results agree with calculations by Azofra et al, who reported that introducing corrugation into the planar g-C_3N_4 reduced its energy by 2.97 eV and its lattice distance to 13.67Å.[34] The bader charge analysis of the flat g-C_3N_4 show that the charge of the carbon and nitrogen atoms are 1.46 and -1.09 respectively.

Table 2: Summary of bond lengths of optimized planar and corrugated g-C_3N_4

Bond	C1-N1	C1-N2	C2-N2	C2-N3
Planar	1.393Å	1.330Å	1.334Å	1.473Å
Corrugated	1.381Å	1.316Å	1.323Å	1.450Å

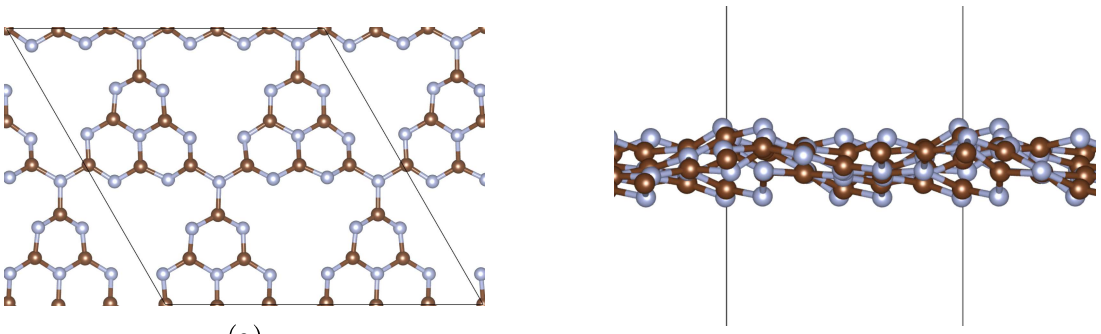

(a) (b)

Figure 4: DFT results of pristine corrugated g-C_3N_4 from two views: (a)Top view (b)Side view

3.2 Doped g-C_3N_4

Using the optimized geometry of pristine g-C_3N_4 from the previous section, doped structures of g-C_3N_4 were modeled by substituting a dopant for one C or N atom. The stability of doped g-C_3N_4 was evaluated from its formation energy, with structures with the lowest energy being most stable.

3.2.1 B-doped g-C_3N_4

The 6 dopant sites C1, C2, I1, N1, N2, N3 considered for Boron doped g-C_3N_4 are shown in Figure 1. The optimized geometries of these sites are shown in Figure 5. The formation energy of each dopant site is shown in Table 3. The formation energy of boron doped g-C_3N_4 was lowest in site C2, where the dopant is substituted into the edge carbon atom. The table also shows that the carbon sites are more stable than other sites due to their low formation energies. Calculations of formation energies by several authors such as Ding, Yu, and Bhagat also agree that C2 is the most stable of the dopant sites considered for this study.[13,35,36]

The Bader Charge analysis of site C2 reveals that the boron atom has a charge of 2.09. This charge was calculated by subtracting the bader charge of the dopant from the number of valence electrons of its single atom. Table 3 also shows that carbon doping sites for boron have a higher charge than nitrogen or interstitial sites. A higher charge for the boron atom

indicates more transfer of electrons between it and the surrounding electronegative nitrogen atom, which thus, could indicate better stability of the system. The boron atom also has a higher charge than a carbon atom in pristine g-C_3N_4. Thus, boron may be an especially reactive site, especially when interacting with negatively charged species.

The bond distance between boron and the surrounding nitrogen atoms was 1.41 Å for B-N2 and 1.50 Å for B-N3. Comparing these values with the bond lengths of plain g-C_3N_4 in table 2 shows that boron doping leaves bond lengths relatively unchanged, with an increase in bond lengths for B-N2 and B-N23 by 0.08 Å and 0.03 Å respectively. The bonding length comparison shows that the bond between boron the surrounding nitrogen atoms are weaker than its carbon equivalent in pristine g-C_3N_4.

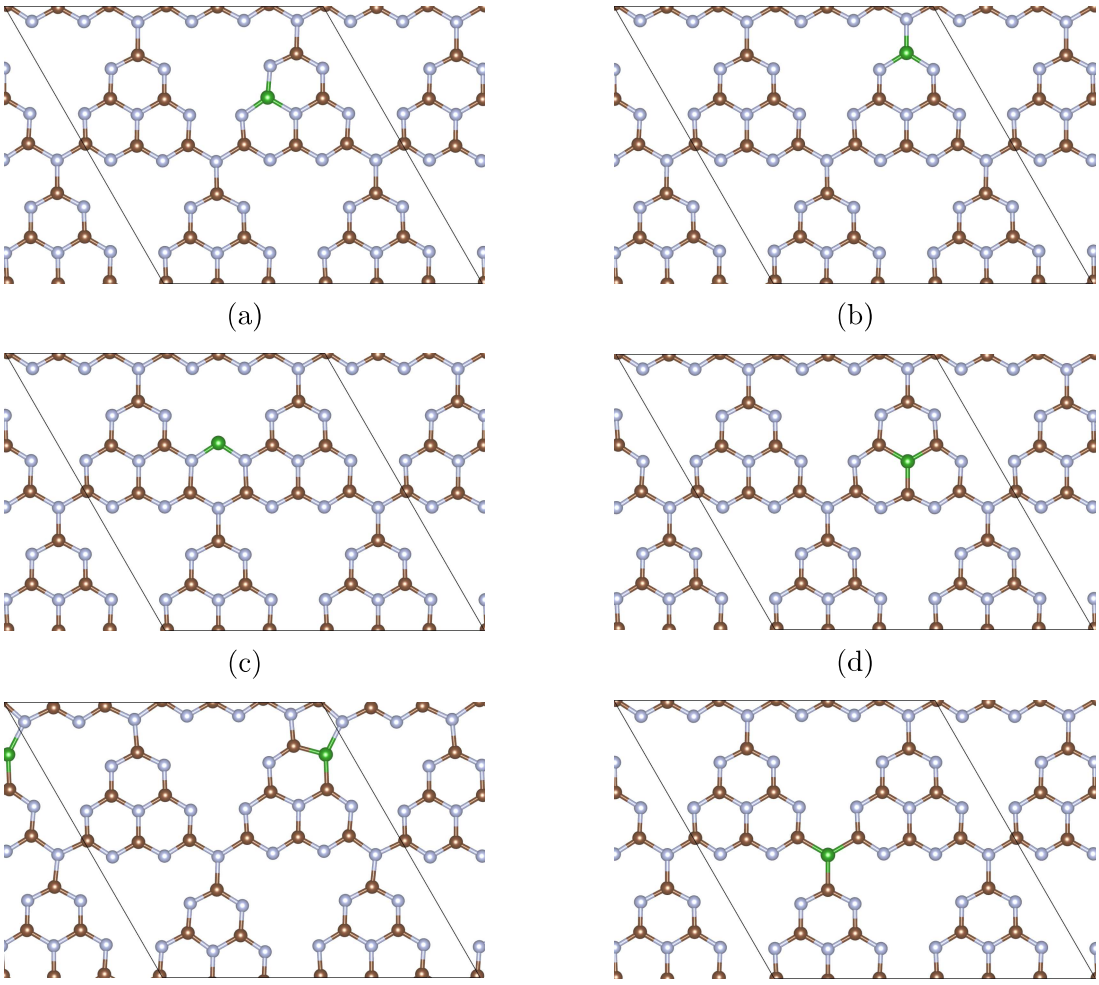

Figure 5: The optimized structures of g-C_3N_4 doped with boron (Green Sphere) in: (a)doping site C1 (b)doping site C2 (c)doping site I1 (d)doping site N1 (e)doping site N2 (f)doping site N3

Table 3: Summary of results for boron doping, including formation energies and charge of dopant atoms.

Dopant	Site	N-Rich E_f (eV)	C-Rich E_f (eV)	Dopant Charge
B	C1	-0.756	-1.55	2.17
B	C2	-1.03	-1.83	2.09
B	I1	7.53	7.53	1.19
B	N1	1.63	2.22	1.78
B	N2	0.246	0.842	1.64
B	N3	1.49	2.08	1.90

3.2.2 S-doped g-C_3N_4

The stability of 6 dopant sites C1, C2, I1, N1, N2, N3 were considered for sulfur doped g-C_3N_4, and their final geometries are shown in Figure 6. The formation energies listed in Table 4 show that the sulfur doped g-C_3N_4 is most stable in site N2, where the atom is substituted into the aromatic nitrogen atom. Previous DFT calculations by Wang et al also report the lowest formation energy at this site.[12] Other computational studies which model sulfur doping on g-C_3N_4 have used a supercell with several stacked sheets. Authors who modeled double stacked layers reported that their lowest energy site is the same as mono-layer g-C_3N_4, with formation energies of 1.17 eV, 1.52 eV report at N2 by Chen and Gao and Stolbov and Zuluaga respectively.[37,38]

Bader Charge analysis of the lowest formation energy structure reveals that the sulfur atom has a charge of 0.10. The positive value of the dopant charge indicates a transfer of electrons from the sulfur dopant to the surrounding atoms when doping occurs. Sulfur as a dopant has the opposite trend of boron doping, where the most stable site also has the least electron transfer. Thus, at first glance, sulfur may not be as reactive as boron upon doping. The perturbations of the electronic structure in C_3N_4 may also not be as strong upon sulfur doping.

The bond length of the sulfur in site N2 and the surrounding carbon atoms were 1.78 Å for S-C2 and 1.73 Å for S-C1. Comparing these value to that of pristine g-C_3N_4 in table 2, we can see that the bond lengths of g-C_3N_4 increase by 0.45 Å and by 0.40 Å. This increase in bond lengths show that the bond between dopant and carbon is unstable for sulfur doped g-C_3N_4 and agrees with our positive formation energy values.

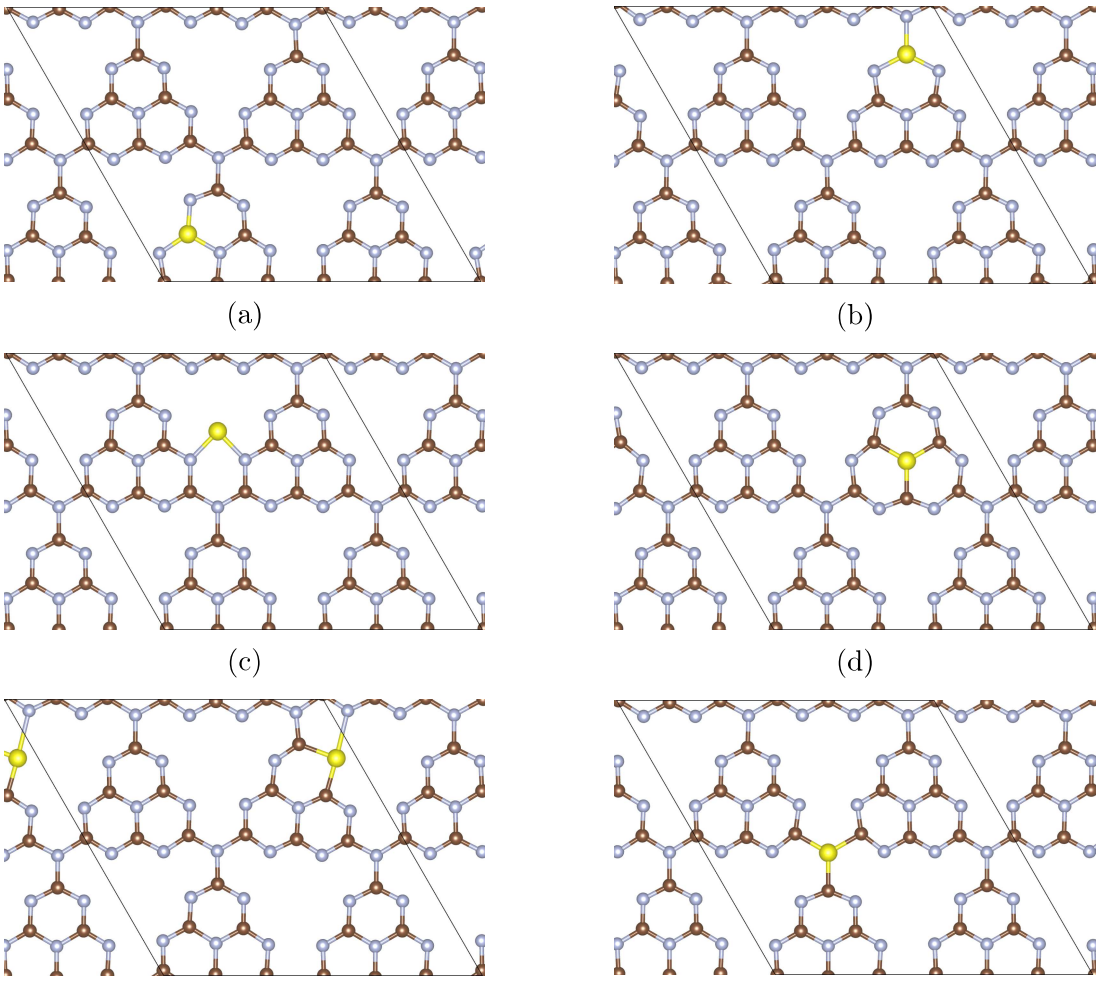

Figure 6: The optimized structure of g-C_3N_4 doped with Sulfur in: (a)doping site C1 (b)doping site C2 (c)doping site I1 (d)doping site N1 (e)doping site N2 (f)doping site N3

Table 4: Summary of Sulfur doped g-C_3N_4 results, including formation energies and Bader charges of dopant atoms.

Dopant	Site	N-Rich E_f (eV)	C-Rich E_f (eV)	Dopant Charge
S	C1	6.29	5.49	2.51
S	C2	5.15	4.36	1.39
S	I1	1.88	1.88	0.81
S	N1	5.84	6.44	0.59
S	N2	1.04	1.63	0.10
S	N3	3.58	4.17	0.48

3.2.3 O-doped g-C_3N_4

The stability of 6 dopant sites C1, C2, I1, N1, N2, N3 were considered for oxygen doped g-C_3N_4 as shown in Figure 7. The formation energy of each dopant site is shown in Table 5. The formation energy for this dopant was lowest in site N2, where the atom is substituted into the aromatic Nitrogen atom. This finding agrees with computational results by Cui, who reported that site N2 has the lowest formation energy of.[39] Experimental results and DFT calculations by Huang also report the lowest formation energy at this site, but for double layer g-C_3N_4.[40] From literature we can see that the only stable site for oxygen doped g-C_3N_4 is site N2 for both its stacked and mono-layer form. Table 7 also shows that site N2 is the only doping site with an oxygen dopant with a negative formation energy. This shows that the oxygen prefers doping on the N2 site due to its stability.

Bader Charge calculations in Table 5 revealed that the doped oxygen atom doped at site N2 have a charge of -0.98. The negative charge of the doped oxygen shows that the dopant gains 0.98 electrons upon doping into g-C_3N_4. In the case of oxygen doping, the electronegative nature of oxygen is different than previous dopant sites and gains electrons from the carbon atoms. Similar to the case of sulfur doped g-C_3N_4, the oxygen is most stable when having its lowest charge due to its electronegativity. This trend is shown in table 5 where site N2 has the lowest charge dopant and the lowest formation energy. The bond lengths between the oxygen dopant and the surrounding nitrogen atoms were 1.36 Å for O-C1 and 1.42 Å for O-C2. The increase in bond lengths of O-C1 and O-C2 compared to results for N2-C1 and N2-C2 in Table 2 show that these bonds are weaker than the N2-C bonds in pristine g-C_3N_4.

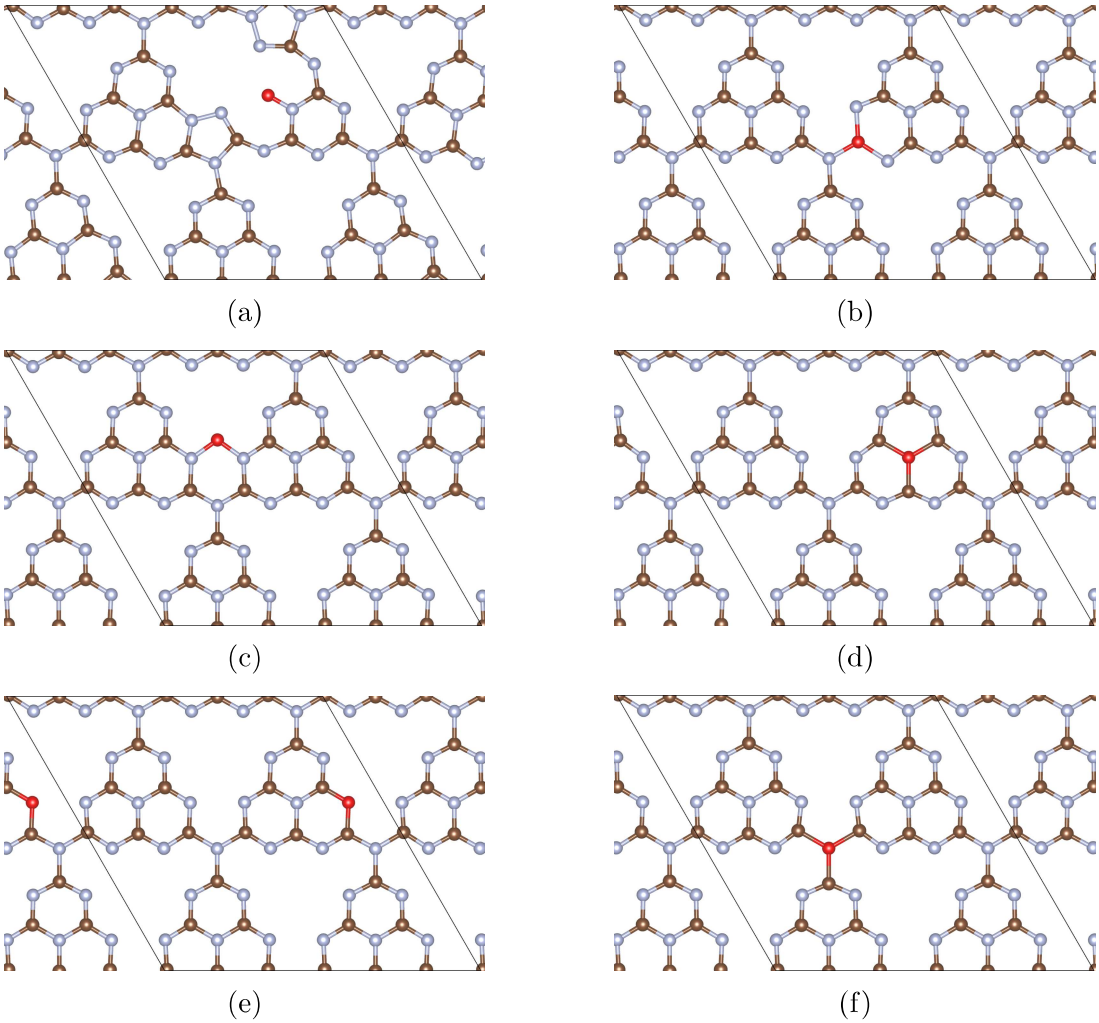

Figure 7: The optimized structure of g-C_3N_4 doped with Oxygen in: (a)doping site C1 (b)doping site C2 (c)doping site I1 (d)doping site N1 (e)doping site N2 (f)doping site N3

Table 5: Summary of oxygen doping results, including formation energies and Bader charges of dopant atoms

Dopant	Site	N-Rich E_f (eV)	C-Rich E_f (eV)	Dopant Charge
O	C1	3.57	2.78	-0.43
O	C2	6.21	5.42	-0.30
O	I1	3.00	3.00	-0.25
O	N1	0.700	1.30	-0.76
O	N2	-0.852	-0.257	-0.98
O	N3	1.40	2.00	-0.77

3.2.4 P-doped g-C_3N_4

The stability of 6 dopant sites C1, C2, I1, N1, N2, N3 were considered for phosphorus doped g-C_3N_4 as shown in Figure 8. The formation energy of each dopant site is shown in Table 6. The formation energy of the Phosphorus was lowest in site I1, where the atom nests in the heptazine pocket of the structure. This result agrees with previous DFT studies from Gorai and Kundu, who found that the interstitial dopant site had the lowest formation energy at -4.079 eV,[29] compared to our value of 0.711 eV. The difference in formation energies could be caused by using different reference states for phosphorus. It is uncertain whether this factor has an effect of the formation energy since the reference state of phosphorus used in Gorai and Kundu's study was not specified. Gorai and Kundu also used a different van Der Waals correction factor (Tkatchenko and Scheffer correction) for geometry optimization which would also produce different energies.

A challenge with phosphorus doping is that many different authors have found differing results. Molaei et al, who calculated the formation energy of doping sites N1 to N3 concluded that the most stable site is N2.[41] Another study by Zheng et al concluded in the most likely dopant site would be site carbon site C1.[42] Ranjbakhsh et al's experimental and computational investigation of the phosphorus doping concluded that is most stable site is in the C2 position.[14] These studies however, didn't calculate the formation energies of all possible doping sites on g-C_3N_4 (including I1). Zheng et al and Ranjbakhsh et al, disregarded the possibility of the most stable site being a nitrogen site because of experimental results. Molaei et al, on the other hand, disregarded the possibility of carbon site for the same reason. Revisiting Table 8 with that knowledge, we can see that our results somewhat agree with Ranjbakhsh et al and Molaei et al as the most stable Carbon doping site is C2, while the most stable Nitrogen doping site is N2 in the table. The difference in our results from Zheng et al could come from their DZVP basis set and Goedecker-Teter-Hutter pseudopotentials.

The Bader Charge analysis of the I1 system reveals that the Phosphorus atom has a charge of 1.03. From comparing bader charges and formation energies if table6, we can see

that there is no clear trend between phosphorus charge and stability. This could indicate that the degree of electron transfer between the dopant and surrounding atoms do not play a role in the stability for Phosphorus doping. The bond lengths of the dopant and nitrogen atoms for site I1 were 1.81 Å for both atoms indicating a weak binding onto the g-C_3N_4.

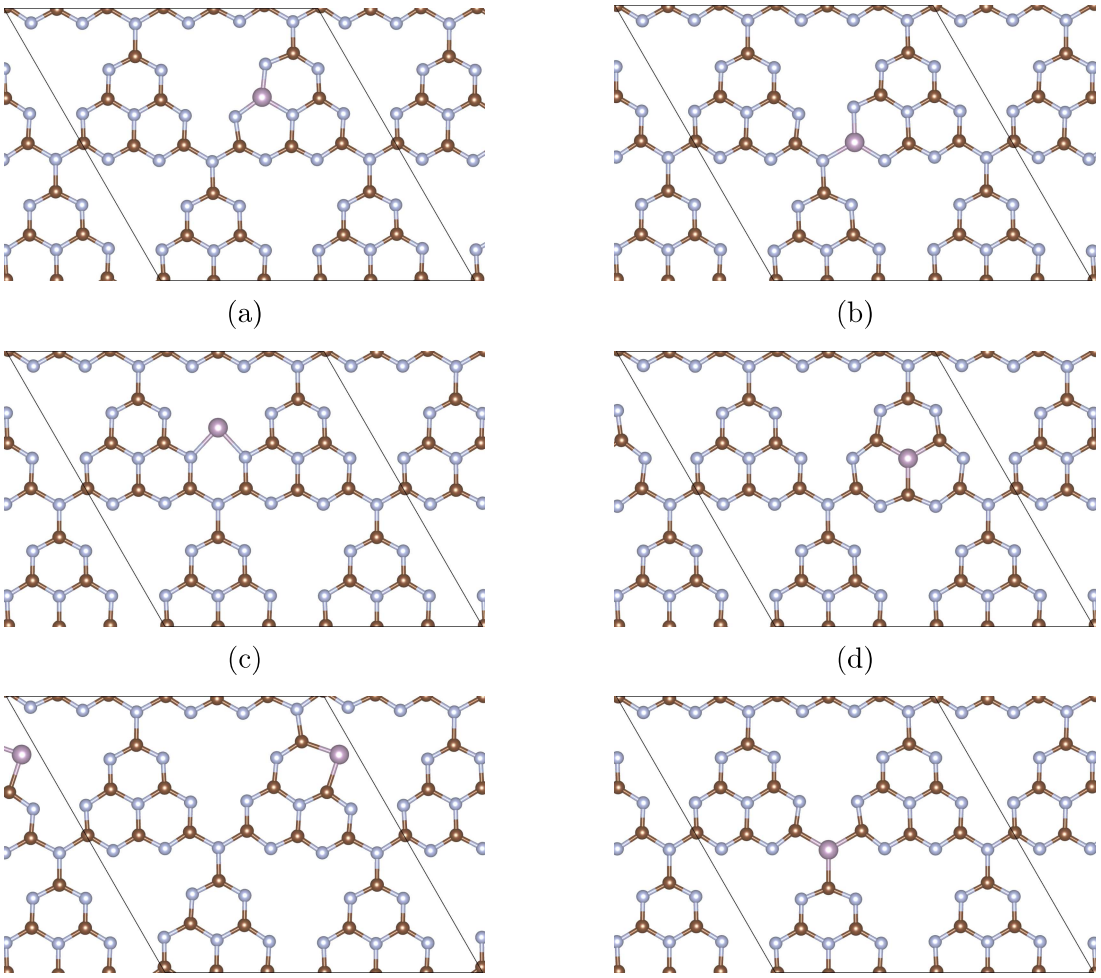

Figure 8: The optimized structures of g-C_3N_4 doped with phosphorus in: (a)doping site C1 (b)doping site C2 (c)doping site I1 (d)doping site N1 (e)doping site N2 (f)doping site N3

Table 6: Summary of phosphorus results, including formation energies and Bader charges of dopant atoms.

Dopant	Site	N-Rich E_f (eV)	C-Rich E_f (eV)	Dopant Charge
P	C1	2.93	2.14	3.30
P	C2	1.96	1.17	2.65
P	I1	0.711	0.711	1.03
P	N1	4.84	5.44	2.25
P	N2	0.972	1.57	1.03
P	N3	4.69	5.29	-0.52

3.3 Cobalt Binding to Doped g-C_3N_4

3.3.1 Cobalt Binding to B-Doped g-C_3N_4

A total of six binding sites of cobalt within the heptazine pocket were considered for this study as shown in Figure 2. The optimized structures for each site are shown in Figure 9 and the adsorption energies in Table 7. The biggest difference among the different binding sites is the coordination number of the cobalt in each site, which dictates the number of atoms it is bonded to. Cobalt atoms have a tendency to converge into the center of the heptazine pocket regardless of initial location. This can be seen in both site A and site B types. This is likely due to the large atomic radius of cobalt, which creates the need for the cobalt atom to maintain a distance larger than 2.1 Å. The most stable cobalt adsorption site of boron doped g-C_3N_4 was site A3, which had an adsorption energy of -4.96 eV and a coordination number of 3. The bond lengths between the cobalt atom and the surrounding nitrogen atoms in boron-doped g-C_3N_4 were 2.08 Å, 2.25 Å and 2.03 Å. Comparatively, cobalt loaded over plain g-C_3N_4 was found to have a coordination number of 4, with longer bond lengths of 2.38 Å, 2.08 Å, 2.08 Å and 2.38 Å. This result is can be further assessed by comparing the adsorption energies of the cobalt atom onto pristine and boron doped g-C_3N_4. The adsorption energy for cobalt on plain g-C_3N_4 was -3.67 eV, which is in agreement to simulations of other authors such as Zhang et al and Guo et al who reported adsorption

energies of -4.01 eV and -3.76 eV.[43,44] The adsorption energy of the cobalt loaded plain g-C_3N_4 has a higher adsorption energy than its Boron doped variant by 1.29 eV. From this comparison, we can see that introducing the boron dopant onto pristine g-C_3N_4 will improve the stability of cobalt adsorption. In this case, both the bond length and adsorption energy comparison indicate that boron doped into g-C_3N_4 is beneficial for stable loading of cobalt onto its structure.

A Bader charge analysis reveals that the cobalt atom on boron doped g-C_3N_4 has a charge of 0.93. We expected that a higher cobalt charge would facilitate more electron transfer between the cobalt and nitrogen atoms and stabilize the structure. This was proven to not be the case, as site B2 in table 7 has a higher cobalt charge than as site A2, but has a lower adsorption energy. Table 7 also shows no correlation between coordination numbers and stability for this system. The cobalt loaded onto pristine g-C_3N_4 has a charge of 0.93, which is similar to that of cobalt on the Boron doped structure. This indicates that the boron atom presents no change in the oxidation state of the cobalt atom.

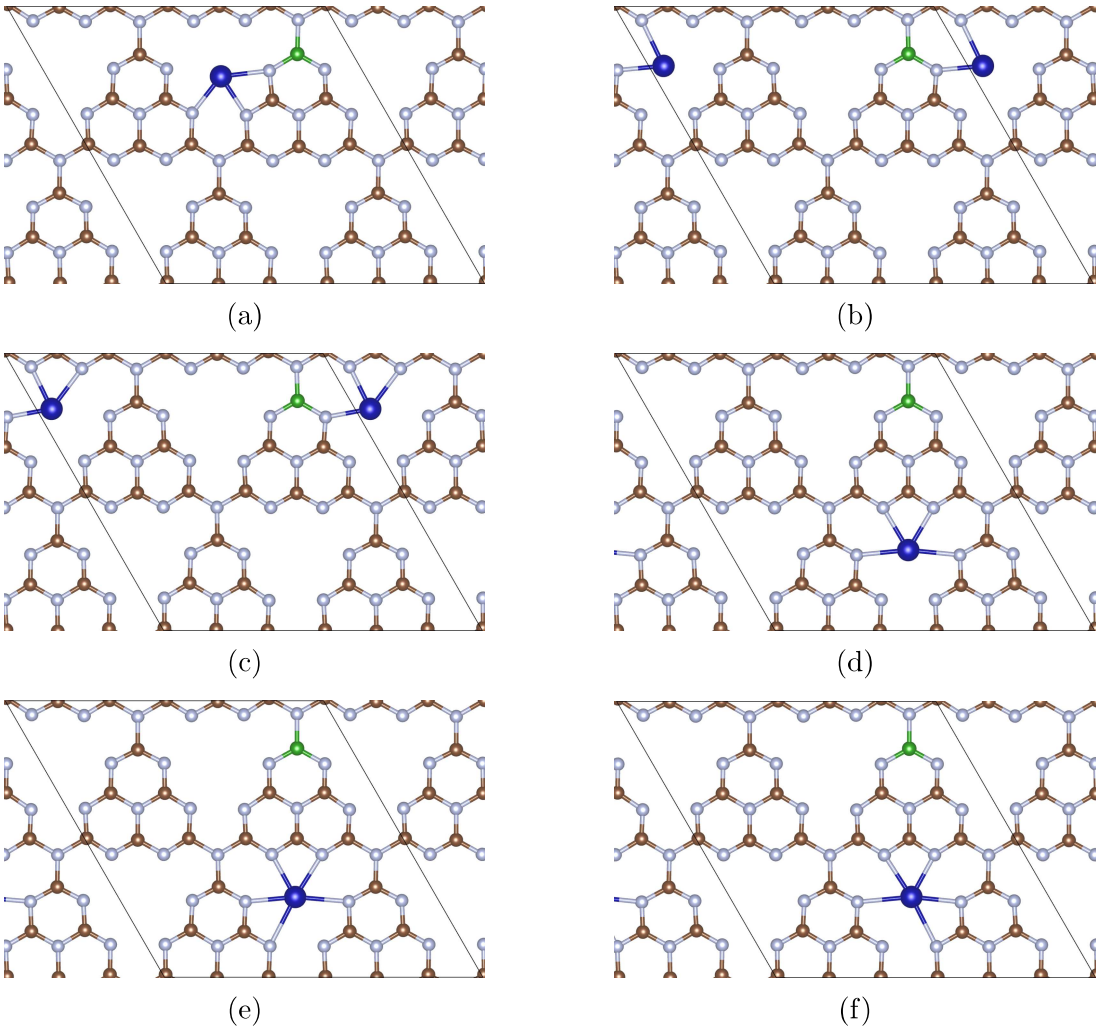

Figure 9: DFT results of Co binding to flat B-doped g-C_3N_4 (green sphere) in: (a) site A1 (b) site A2 (c) site A3 (d) site B1 (e) site B2 (f) site B3

Table 7: Summary of adsorption energies for each Cobalt site considered for flat boron doped g-C_3N_4. Coordination numbers and cobalt charges are also provided.

Dopant	Site	E_{Ads} (eV)	Coordination Number	Cobalt Charge
B	A1	-4.95	4	0.94
B	A2	-4.93	4	0.88
B	A3	-4.96	3	0.93
B	B1	-4.57	4	0.86
B	B2	-4.58	5	0.91
B	B3	-4.58	5	0.86

3.4 Effects of Corrugation on Doping and Cobalt Adsorption

3.4.1 Effects of Corrugation on Doped g-C_3N_4

Previous studies investigating transition metal doping on g-C_3N_4 through DFT have observed that the lowest energy structures tend to be corrugated.[16,45–47] One difference between corrugated and planar g-C_3N_4 is the decrease in the total energy of carbon nitride sheets by 2.91 eV as seen from Azofra et al.[34] From this finding, it would be reasonable to expect doped g-C_3N_4 to have a lower energy and reduced cell size upon corrugation. Table 8 shows the formation energies for the planar and corrugated structure for each dopant. The corrugated structures doped with boron have a lower formation energy than their planar counterparts, while sulfur doped and oxygen doped structure show the opposite trend. The most stable site for flat Oxygen doped g-C_3N_4 is the same as its corrugated phase. The most stable site for flat Sulfur doped g-C_3N_4 is also the same for its corrugated phase. The most stable site of Boron doped g-C_3N_4 changed from site C2 to site C1 when corrugated.

The Bader charge analysis reveals the charge of the dopant for boron doped g-C_3N_4 is similar in both its flat and corrugated phases. From this information, it can be inferred that corrugation has little effect on the electron transfer between the dopant and surrounding atoms. This eliminates the possibility of the change in the most stable doping site for boron doped g-C_3N_4 being due to distribution of charge. The consistency in the charge of the cobalt atom after corrugation could also mean that the number of electrons which take part the in the CO_2 reduction reaction is the same for planar and corrugated structures. A reason for the change in the most stable site could be due to corrugation could be the reduction in cell size by 0.44 Å that the boron doped g-C_3N_4 experiences upon corrugation. The distances between the dopant and its surrounding atoms for corrugated boron doped g-C_3N_4 change to 1.47 Å and 1.31 Å. Compared to the bond distances of its flat variant, the bond lengths of the corrugated boron g-C_3N_4 are shorter by 0.03 Å and 0.1 Å respectively. This shortening of the bond length is could be the reason that the corrugated boron doped is more stable

than its planar form.

Table 8: Summary of formation energies, Bader charges, and lattice parameters of plain and doped g-C_3N_4 for flat and corrugated sheets.

Dopant	State	Site	E_f (eV)	Lattice Parameter(Å)	Dopant Charge
B	Planar	C2	-0.756	14.26 Å	2.17
B	Corrugated	C1	-1.59	13.82 Å	2.16
S	Planar	N2	1.04	14.26 Å	0.10
S	Corrugated	N2	1.63	13.76 Å	0.24
O	Planar	N2	-0.852	14.26 Å	-1.00
O	Corrugated	N2	-0.257	13.74 Å	-1.00

3.4.2 Cobalt Loading on Corrugated Boron Doped g-C_3N_4

Similar to the case of flat Boron doped g-C_3N_4, a total of six sites were considered for Cobalt loading on corrugated g-C_3N_4. Table 9 shows that the Cobalt site with the lowest adsorption energy for corrugated g-C_3N_4 was site A1, of which the most stable structure is shown in Figure 10. The corrugated Boron doped Cobalt loaded g-C_3N_4 is less stable in site B. The overall average adsorption energy is lower for corrugated Boron doped Cobalt loaded g-C_3N_4, indicating the binding of the Cobalt on the surface is weaker than its planar counterpart. This was likely brought about because of the shrinking of the distance between the Cobalt atom and the surrounding Nitrogen atoms. Overall, boron doping on g-C_3N_4 stabilizes cobalt loading for both planar and corrugated structures. This would mean stronger binding of cobalt onto the boron doped g-C_3N_4, which could increase the lifetime of cobalt loaded boron doped g-C_3N_4 as a photocatalyst. Corrugation of the g-C_3N_4 sheet also weakens the cobalt binding, but does not bring any change to the cobalt charge. This result indicates that corrugation on cobalt loaded boron doped g-C_3N_4 hinders it as a photocatalyst due to its weak cobalt binding.

Table 9: Summary of adsorption energies for each Cobalt loading site on corrugated Boron doped g-C_3N_4.

Dopant	Site	$E_(Ads)$ (eV)	Coordination Number	Cobalt Charge
B	A1	-4.98	2.14	0.91
B	A2	-4.94	1.17	0.91
B	A3	-4.98	0.711	0.92
B	B1	-4.87	5.44	0.83
B	B2	-4.87	1.57	0.88
B	B3	-4.87	5.29	0.86

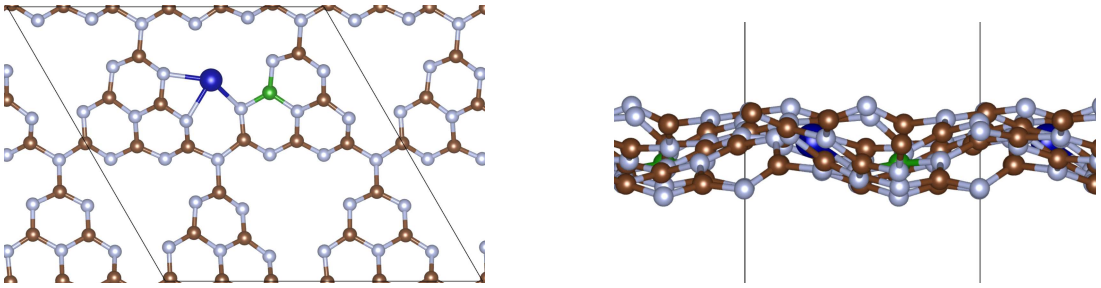

(a) (b)

Figure 10: DFT results of Co binding on corrugated B-doped g-C_3N_4. (a)Front view of result from lowest E_{Ads} site A3. (b)Side view of result from lowest E_{Ads} site A3.

3.5 Carbon Dioxide Adsorption onto Corrugated Co-B g-C_3N_4 Structures

Carbon dioxide adsorption onto the cobalt loaded boron doped g-C_3N_4 was also modeled after the most stable Cobalt resting site was found, of which results are in Table 10. All CO_2 adsorption sites that we modeled in for cobalt loaded boron doped g-C_3N_4 did not result in the bent CO_2 structure commonly seen in CO_2 reduction for cobalt loaded g-C_3N_4.[44] The site with the lowest adsorption energy is shown in Figure 11. The Figure shows that the CO_2 molecule prefers to adsorbs onto the surface in a vertical orientation. The adsorption energy for this configuration of CO_2 on cobalt loaded boron doped g-C_3N_4 was -0.24 eV, which indicates a stable structure.

Table 10: Summary of adsorption energies for CO_2 adsorption on corrugated g-C_3N_4.

Dopant	E_{Ads} (eV)
None	-0.60
Boron	-0.39
Cobalt-Boron	-0.24

Literature on carbon dioxide adsorption by Xia reported that CO_2 adsorbs onto a g-C_3N_4 surface with an adsorption energy of -1.37 eV.[48] The adsorption energies of carbon dioxide on corrugated g-C_3N_4 in our model was comparatively less stable at -0.60 eV. This difference in adsorption energy could be due to different geometries in the two works. Xia et al's planar model was less corrugated than our model, and it is unclear if their initial C_3N_4 sheet before CO_2 adsorption was flat or corrugated. For comparison with the pristine model, a model of CO_2 adsorption on corrugated cobalt loaded g-C_3N_4 was also calculated. This model had an adsorption energy of -0.24 eV. Studies on cobalt loaded g-C_3N_4 by Ao et al and Guo et al found CO_2 adsorption energies of -0.83 eV and -0.81 eV respectively.[15,44] The model for cobalt loaded g-C_3N_4 in the current study likely has a higher energy compared to literature values due not being at the lowest energy configuration. More trials could reveal a lower energy structure with adsorption energy values which match that of Ao et al and Guo et al. There is also the possibility of different simulation setting affecting the adsorption energy of CO_2 on g-C_3N_4. Ao et al used the D2 van Der Waals correction factor in their calculations, which would give different adsorption values than the D3 method we used.[15] Guo et al also simulated CO_2 adsorption and included the effect of water in their model through an implicit solvation model.[44]

One trend found in both the adsorption energies from this study and literature values is that the binding of CO_2 on g-C_3N_4 is weakened with the addition of cobalt. Comparing adsorption energy from our cobalt loaded boron doped g-C_3N_4 to literature values suggests that this binding weakens even further with the addition of the boron dopant. The CO_2 adsorbed onto the cobalt loaded boron doped g-C_3N_4 was around 3.22 Å from the cobalt

atom. The distance between the cobalt and CO_2 from Ao et al was 1.76 Å[15] which is much shorter than our obtained values. This comparison shows that the bond distance is a contributor to the high adsorption energy of our model. Overall, boron doping combined with a cobalt site is not beneficial for CO_2 adsorption, but is still able to weakly bind the CO_2 molecule to the cobalt atom. Both the boron dopant and the cobalt loading both contribute to this weak binding. This is due to the boron doping itself increasing the adsorption energies of g-C_3N_4, even without the effects of cobalt.

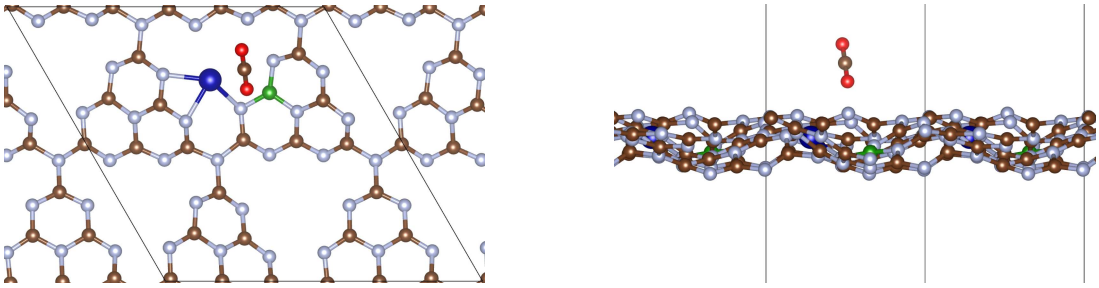

(a) (b)

Figure 11: DFT results of Co binding on corrugated B-doped g-C_3N_4. (a)Front view of result from lowest E_{Ads} for CO_2 on Cobalt loaded Boron doped g-C_3N_4 (b)Side view of result from lowest E_{Ads} for CO_2 on Cobalt loaded Boron doped g-C_3N_4

3.6 Band Gap and Density of States of g-C_3N_4

3.6.1 Band Gap and Density of States Calculations using the PBE Functional

The density of states (DOS) and band gap was determined for the most stable site of each dopant type. Table 11 shows the band gap of each structure calculated with the PBE functional. It is well established that the LDA functional and by extension, the GGA functional, tends to underestimate the band gap of semiconductors.[49] Calculations on pristine g-C_3N_4 by Li et al[46] and Tran et al[11] have shown that the PBE functional underestimates the band gap of g-C_3N_4 by 1.13 to 1.88 eV compared to the experimental value of 2.7 eV,[6] which agrees with our results as shown in Table 11.

The same table shows that compared to its pristine counterpart, flat g-C_3N_4 doped with

Table 11: Summary of band gaps of planar and corrugated doped g-C_3N_4 calculated using the PBE functional.

Dopant	Phase	Dopant Site	Band Gap (eV)
None	Planar	None	1.20
None	Corrugated	None	1.62
Boron	Planar	C2	1.16
Boron	Corrugated	C1	1.77
Sulfur	Planar	N2	1.14
Sulfur	Corrugated	N2	1.77
Oxygen	Planar	N2	1.21
Oxygen	Corrugated	N2	1.87
Cobalt-Boron	Planar	C2	1.08
Cobalt-Boron	Corrugated	C2	1.61

Boron, and Sulfur have slightly smaller band gaps, while the band gap of Oxygen doped g-C_3N_4 is remains about the same. The smaller band gap of flat g-C_3N_4 doped with boron or sulfur allows the material to absorb light with lower energies and longer wavelengths. This gives these two materials an advantage as a photocatalyst compared to pristine g-C_3N_4 as they can absorb a wider range of light.

A study of corrugated Oxygen doped g-C_3N_4 by Tran et al showed that Oxygen doped reduced the band gap from 1.88 eV to 1.75 eV while our results show the opposite trend.[11] This difference in results could come from a difference in the corrugation pattern of the Oxygen doped g-C_3N_4. DOS calculations of planar Sulfur doped g-C_3N_4 from Wang et al show that it has a smaller band gap than its pristine form, which agrees with trends from Table 11. Band gap values also from Table 11 show that cobalt loading narrows the band gap of doped g-C_3N_4. This is true for both planar and corrugated boron doped g-C_3N_4, which experienced a band gap decrease by 0.08 eV and 0.16 eV respectively. It can also be observed that the band gap for corrugated cobalt loaded boron doped g-C_3N_4 is wider than its planar equivalent. This agrees with the pattern that corrugating g-C_3N_4 generally widens band gap and thus hinders light adsorption on g-C_3N_4. Finally, it can also be observed that corrugation will increase the band gap by 0.59 eV of doped and pristine g-C_3N_4 on average. This agrees

with previous results where corrugation increases band gaps.[50] From this observation, we can infer that effect of corrugation on the band gap of g-C_3N_4 is not desirable for CO_2 reduction. This would be due to the enlargement of the band gap caused by corrugation, which would hinder the electrons ability to absorb light with longer wavelengths.

The density of states results of each variation of flat g-C_3N_4 are shown in Figure 12 in plots a, c, e and g. From Figure 12c and d, we can see that unoccupied states exist above the Fermi energy inside the band gap for both planar and corrugated Boron doped g-C_3N_4 in the spin down configuration. The Oxygen/Sulfur doped g-C_3N_4 also has defect states similar to the Boron doped variant, but which are occupied due to being under the Fermi energy. These defect states within the band gap effectively lower the energy required for electrons to energize into the conductance band and allow for better usage of light for photo-catalysis. The density of states plot also shows that the Fermi level shifted near the conductance band for Oxygen and Sulfur doping g-C_3N_4. This shows that doping g-C_3N_4 with Oxygen and Sulfur produces a n-type semiconductor.

The partial density of states of planar and corrugated Boron doped g-C_3N_4 in Figure 12 shows that the defect states near the valence band of doped g-C_3N_4 are mostly comprised of electrons of the Nitrogen atom. The defect states of sulfur doped g-C_3N_4 and oxygen doped g-C_3N_4, on the other hand, are comprised of equal contribution from electrons from the nitrogen and carbon atom. From this finding we expect the electrons from the carbon atoms to be more likely to become energized and take part in the CO_2 reduction reaction for oxygen and sulfur doped systems. Figure 12 shows that the planar and corrugated density of states plot for doped g-C_3N_4 are similar in shape. One trend that can be found from comparing these two variants is that the defect state of doped corrugated system is better separated from the band it is closer to. This would reduce the amount of energy required for an electron in that defect state to move into another band.

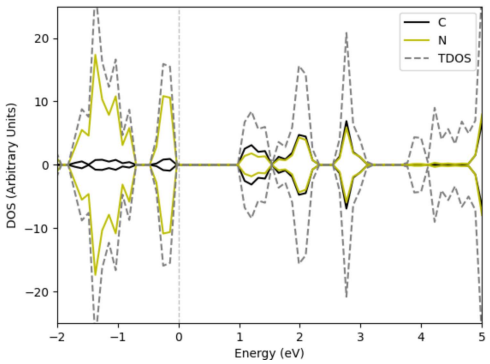
C
N
TDOS
DOS (Arbitrary Units)
Energy (eV)

(a)

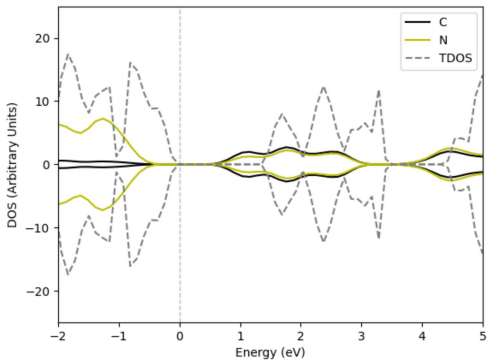
C
N
TDOS
DOS (Arbitrary Units)
Energy (eV)

(b)

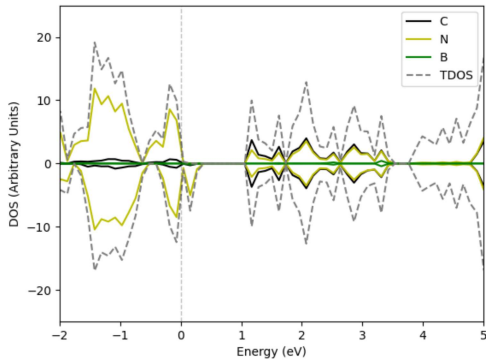
C
N
B
TDOS
DOS (Arbitrary Units)
Energy (eV)

(c)

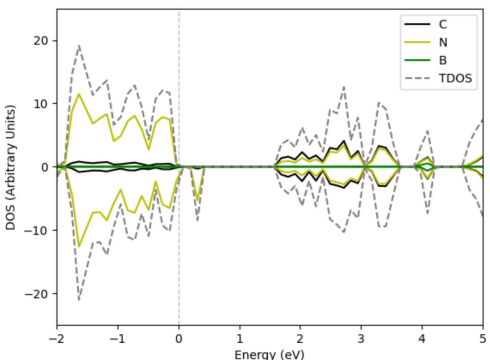
C
N
B
TDOS
DOS (Arbitrary Units)
Energy (eV)

(d)

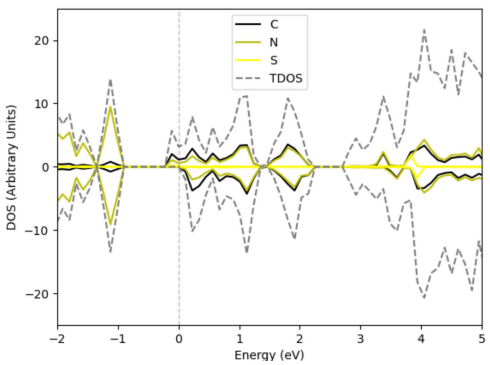
C
N
S
TDOS
DOS (Arbitrary Units)
Energy (eV)

(e)

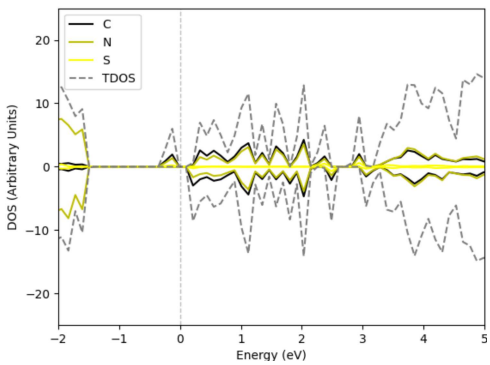
C
N
S
TDOS
DOS (Arbitrary Units)
Energy (eV)

(f)

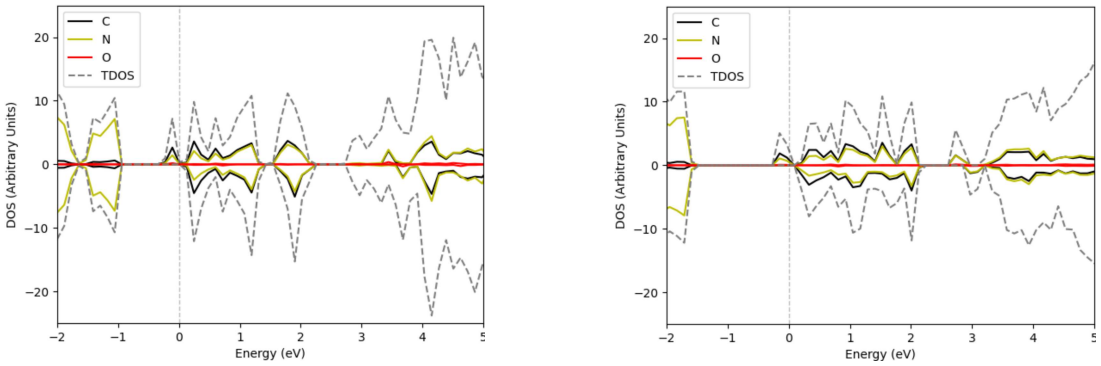

(g) (h)

Figure 12: Density of states plots of different doped g-C_3N_4 systems using the PBE functional with the Fermi energy set at 0 eV. The structures represented here are for: (a)Flat Pristine g-C_3N_4 (b)Corrugated Pristine g-C_3N_4 (c)Flat Boron doped g-C_3N_4 (d)Corrugated Boron doped g-C_3N_4 (e)Flat Sulfur doped g-C_3N_4 (f)Corrugated Sulfur doped g-C_3N_4 (g)Flat Oxygen doped g-C_3N_4 (h)Corrugated Oxygen doped g-C_3N_4

The density of states and band gap of adsorption site A3 for corrugated and planar Boron doped g-C_3N_4 were calculated with the PBE functional as shown in Figure 13. The addition of a Cobalt atom decreases the overall band gap of the planar system to 1.08 eV and the corrugated system to 1.61 eV. As seen in the previous section the band gap of corrugated doped systems are generally larger than their planar counterparts. From the comparison of band gaps of planar and corrugated structures of cobalt loaded boron doped g-C_3N_4, this trend is also valid for this for this system as well. The band gap of the two systems both spans from the state around -1.3 eV which we designate as the valence band, to the state around 0.2 eV which we designate as the conduction band. For both structures, the peaks with states in only one spin such as the peak near -0.5 eV and -0.2 eV are counted as defect states which exist inside the band gap. Compared to its doped variant, the cobalt loaded boron doped g-C_3N_4 adds an additional defect state at -0.2 eV near the conductance band. While the defect state near the valence band is occupied by electrons of the nitrogen and cobalt atom, the new state near the Fermi energy is occupied mostly by electrons which belong to the Cobalt atom. This indicates that the electrons of Cobalt are the most likely to take part in photo-catalysis. This would be due to the cobalt atoms within this defect state

being energized to the conductance band with a minimal amount of energy, which indicates that these electrons will be able to absorb light at longer wavelengths. The Fermi energy of the material moved near the conduction band, which indicates that the addition of Cobalt changed the Boron doped g-C_3N_4 into a n-type semiconductor. Similar to the case for oxygen and sulfur doped g-C_3N_4, the band gap of this semiconductor spans from the conductance band at 0.1 eV, past the Fermi level, to the valence band at around -1 eV, and also ignores the two peaks near -1.3 eV and within the band gap. The density of states plot and the band gap of cobalt loaded boron doped g-C_3N_4 shows that both its planar and corrugated phase has two distinct advantages over its non loaded variants. The first is the decreased band gap as can be seen from the band gap values from Table 11 and in this section. The second is the introduction of a defect state near the conductance band comprised of electrons of the cobalt atom. These two changes allow for the cobalt loaded boron doped g-C_3N_4 to use a wider range of light for photocatalysis as explained in this section.

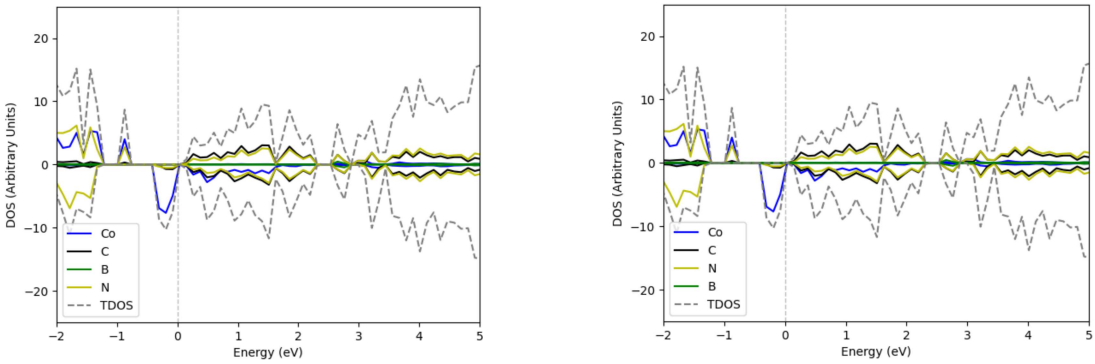

(a) (b)

Figure 13: Density of states plot for Cobalt loaded Boron doped g-C_3N_4 with the Fermi energy set to 0 eV. The plot a is the density of states plot for flat cobalt loaded boron doped g-C_3N_4, while b is the same plot for its corrugated varient

3.6.2 Comparison of the HSE06 and PBE Functionals in Calculating Band Gaps

To compare how the choice of the exchange-correlation functional affects the electronic properties of doped systems, the band gap and DOS of Boron doped g-C_3N_4 were calculated with the HSE06 and PBE functional. It has been well established that the PBE functional under-

estimates the band gap of semiconductors compared to the HSE06 functional.[29,51] Results from authors such as Li et al[46] and Tran et al[11] show that this trend also applies to g-C_3N_4. Their calculations on pristine g-C_3N_4 with the PBE functional returned a band gap of 1.13[46] to 1.88 eV,[11] while the experimental value is 2.7 eV.[6] Azofra et al conducted calculations of the band gap of g-C_3N_4 by using the HSE06 functional and calculated a band gap of 2.71 eV.[34] This value is much closer to the experimental band gap of 2.7 eV by Wang et al.[6] As shown in Table 12, the HSE06 functional gives a band gap of 2.81 eV for pristine g-C_3N_4 for our calculations. Comparing this value to the band gap of flat pristine g-C_3N_4 in Table 11 confirms that the HSE06 functional gives a band gap closer to the experimental value compared to the PBE functional in our models as well.

Although the PBE functional severally mistakes the band gap of g-C_3N_4, it could still prove useful in simulating how doping and corrugation effect the band gap of g-C_3N_4. Table 12, shows that the band gap of planar pristine g-C_3N_4 decreases with boron doping by 0.11 eV, and shows the same for corrugated g-C_3N_4 but by 0.1 eV. The PBE functional results in Table 11 produces the same trend as the results as the HSE06 functional for planar g-C_3N_4, but with a smaller decrease in band gap (0.04 eV). The PBE functional, however, also calculates that the band gap for corrugated g-C_3N_4 will widen upon boron doping by 0.15 eV, which is the opposite trend of the HSE06 results. This comparison shows that the PBE functional is not an accurate in simulating the increase or decrease in band gap of corrugated g-C_3N_4 from doping. The change in band gap for corrugated g-C_3N_4 needs to be recalculated with the HSE06 functional and compared with the results in Table 12 for verification. The density of states plots of the structures calculated with the HSE06 functional are shown in Figure 14. The figure shows that doping the planar and corrugated g-C_3N_4 with Boron lowers the energy of the conductance band, while the valence band remains near the Fermi level as seen in p-type semiconductors. This change can also be observed from the boron doped g-C_3N_4 calculated in Figure 12. The HSE06 functional calculations also show that there are defect states in the band gap near 1 eV, which are comprised of electrons of nitrogen atoms.

Comparing these features with those from the boron doped g-C_3N_4 in Figure 12 shows that the PBE functional was successful in calculating existence of defect states, but not their energies. Overall, the PBE functional cannot accurately quantify the changes in the band gap that occurs from doping g-C_3N_4; however, the characteristics of the density of states plot, such as the existence of defect states and changes in the valence band or conductance band are in line with the accuracy of the HSE06 functional.

Table 12: Summary of Band Gap of Planar and Corrugated Boron Doped g-C_3N_4 Calculated using the HSE06 Functional.

Dopant	Phase	Dopant Site	Band Gap (eV)
None	Planar	None	2.81
None	Corrugated	None	2.90
Boron	Planar	C2	2.70
Boron	Corrugated	C1	2.89

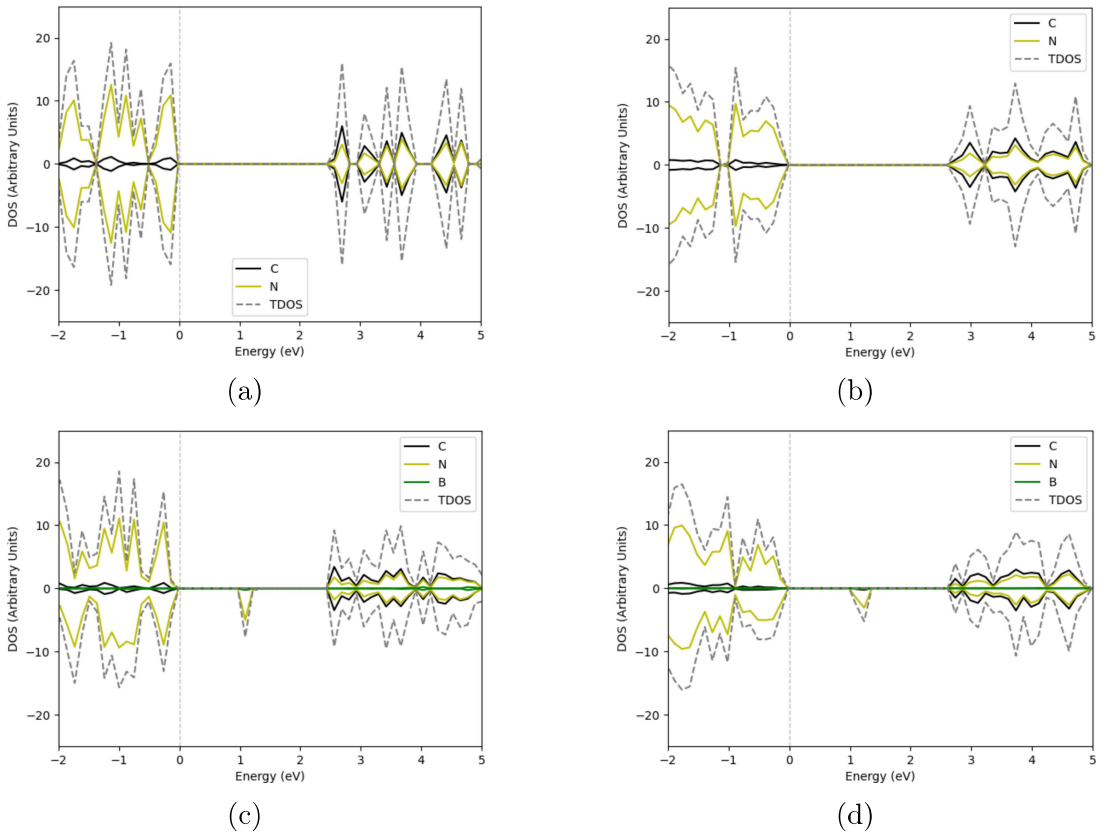

Figure 14: Density of states plots of different doped g-C_3N_4 structures using the HSE06 functional. The Fermi energy is set to 0 eV. The structures represented here are: (a)Flat pristine g-C_3N_4 (b)Corrugated pristine g-C_3N_4 (c)Flat Boron doped g-C_3N_4 (d)Corrugated Boron doped g-C_3N_4

4 Conclusions

In this project, the geometries and density of states of doped g-C_3N_4 was modeled using DFT calculations. Our model of planar and corrugated g-C_3N_4 confirmed that corrugated g-C_3N_4 has a lower total energy and is more stable than its planar variant. Comparison of formation energies across different dopant species and doping sites resulted in the most stable doping sites being site C2 for Boron, N2 for Oxygen and Sulfur. The most stable sites of each dopant followed a trend in which more electronegative dopants preferred to substitute nitrogen sites, while less electronegative dopants were stable in carbon sites. This was due to the electronegative dopants being stable when bonded with carbon, which is less

electronegative than nitrogen. Only the flat phase of Phosphorus doped g-C_3N_4, which was most stable at site I1, was modeled due to time constrains. The stability of Cobalt adsorption onto the Boron doped g-C_3N_4 was evaluated based on its adsorption energy. It was found that the site with the lowest adsorption energy (site A3) is thermodynamically stable because of its negative adsorption energy. From this structure, adsorption of Carbon Dioxide was also modeled onto the surface, which revealed that the adsorption energy of carbon dioxide onto cobalt loaded boron doped g-C_3N_4 was more unstable than cobalt loaded g-C_3N_4 or pristine C_3N_4. The boron doped into g-C_3N_4 would hinder CO_2 adsorption onto the cobalt atom, and thus hinder its abilities as a photocatalyst.

The density of states were calculated for planar and corrugated g-C_3N_4 doped with Boron, Oxygen and Sulfur using the PBE functional. These results showed that doping decreases the band gap for planar g-C_3N_4 but increases it for the corrugated phase. Corrugated g-C_3N_4 was also shown to have a large band gap than its planar variant for all dopants. Results from the density of states calculations for Cobalt loaded Boron doped g-C_3N_4 show that adding elements into the g-C_3N_4 structure through doping or Cobalt adsorption adds a defect state inside the band gap. The band gap of pristine and Boron doped g-C_3N_4 was also calculated from the HSE06 functional and compared with PBE results. This comparison revealed that although the PBE functional underestimates the band gap by a significant margin (1.1 eV) the general characteristics of the density of states plot agree with results using the HSE06 functional. These results point to the conclusion that doping g-C_3N_4 with Boron, Oxygen and Sulfur makes the electronic properties more suited for CO_2 reduction by introducing defect states into the band gap in which electrons could energize to and from.

Adding a Cobalt atom onto Boron doped g-C_3N_4 also proves to be beneficial due to the it addition of another defect state. The opposite is true for corrugated g-C_3N_4, where the band gap becomes larger compared to its planar variant. Overall, boron doping and cobalt loading on g-C_3N_4 was found to be beneficial for carbon dioxide reduction by narrowing and introducing defect states into its band gap. The boron doping and cobalt loading introduces

one drawback, however, in that the binding of CO_2 onto the g-C_3N_4 surface becomes weaker with doping, and Co loading. Doping g-C_3N_4 with sulfur was found to decrease the band gap while oxygen doping was found to increase it. These findings should be reproduced with the HSE06 functional for more accuracy. Corrugation of g-C_3N_4 was overall found to hinder g-C_3N_4 despite its lower energy compared to its planar variant. This is due to the process widening the band gap of g-C_3N_4, while introducing no new characteristics in the density of states.

4.1 Future Work

There are several possible areas where future work could expand upon this project. First, cobalt loading could be modeled on the other dopants modeled in this projects such as Sulfur, Oxygen and Phosphorus. The corrugated phase of Phosphorus doped g-C_3N_4 could also be modeled and compared with its flat variant. Second, structures of corrugated g-C_3N_4 with a lower energy than the ones modeled in this project could be found with further iterations. This is due to there being many geometries in which the corrugated structure to converge to. As an example, the total energy of a corrugated doped system could be dependent on whether the g-C_3N_4 was corrugated or doped first. In this study, the non-metal atoms were substituted into g-C_3N_4 which was pre-corrugated in its pristine form. The total energy of this system could change if we reversed this order, and corrugated planar doped g-C_3N_4 to produce the final structure. Further methods of corrugation could be tested to produce different structures. Due to the number of patterns that g-C_3N_4 can converge to, corrugating different atoms to different degrees could produce structures with different energies. Other considerations for the lowest energy structure which could be considered include the size of the supercell used, and the size of KPOINTS mesh used. If a lower energy corrugated structure were to be found, its properties such as the density of states and band gap could be different from the structures modeled in this project. Third, more geometries of Carbon Dioxide adsorption on Cobalt loaded Boron doped g-C_3N_4 could be modeled to

find a lower energy structure with a bent CO_2 configuration. Other properties of the our structures could also be calculated such as its band structure and intermediate reaction products for CO_2 reduction. For more long term projects, additional dopants for g-C_3N_4 and addition transition metals for loading could evaluated for their effect on the efficiency of CO_2 reduction. These results would then be used to identify properties of doped g-C_3N_4 which are beneficial for photo-catalysis to be used for screening of carbon nitride materials.

Acknowledgement

The authors thank Professor Aaron Deskins for his mentorship and support over the span of the two years during which this project was conducted. Professor Deskins has introduced us to the expansive field of computational modeling, and through his guidance, helped us grow as students and as scientists entering the academic research environment. We are thankful for his sharing of expertise in his field of computational modeling and for introducing us to the wonderful members of the Deskins lab. The authors also thank Qian Qian for her guidance throughout the g-C_3N_4 project. Her discussions on progress and potential solutions to roadblocks, as well as her revisions on our posters and reports have been essential to the completion of this MQP. Finally, we thank Emily Sutherland for providing and editing of the Python code used in this project, as well as her help interpreting the density of states graphs. The authors thank Mats Dahlgren for version one of achemso, and Donald Arseneau for the code taken from cite to move citations after punctuation. Many users have provided feedback on the class, which is reflected in all of the different demonstrations shown in this document.

References

(1) Organization, W. M. *WMO Provisional State of the Global Climate 2022*; 2023; p 26.

(2) Li, K.; Peng, B.; Peng, T. Recent advances in heterogeneous photocatalytic CO2 conversion to solar fuels. *Acs Catalysis* **2016**, *6*, 7485–7527.

(3) Wu, J.; Huang, Y.; Ye, W.; Li, Y. CO2 reduction: from the electrochemical to photochemical approach. *Advanced Science* **2017**, *4*, 1700194.

(4) Galushchinskiy, A.; González-Gómez, R.; McCarthy, K.; Farrás, P.; Savateev, A. Progress in Development of Photocatalytic Processes for Synthesis of Fuels and Organic Compounds under Outdoor Solar Light. *Energy & Fuels* **2022**, *36*, 4625–4639.

(5) Ma, D.; Li, X.; Wang, X.; Luo, Y. Research development on graphitic carbon nitride and enhanced catalytic activity on ammonium perchlorate. *RSC advances* **2021**, *11*, 5729–5740.

(6) Wang, X.; Maeda, K.; Thomas, A.; Takanabe, K.; Xin, G.; Carlsson, J. M.; Domen, K.; Antonietti, M. A metal-free polymeric photocatalyst for hydrogen production from water under visible light. *Nature materials* **2009**, *8*, 76–80.

(7) Dong, G.; Zhang, L. Porous structure dependent photoreactivity of graphitic carbon nitride under visible light. *Journal of Materials Chemistry* **2012**, *22*, 1160–1166.

(8) Wen, J.; Xie, J.; Chen, X.; Li, X. A review on g-C3N4-based photocatalysts. *Applied surface science* **2017**, *391*, 72–123.

(9) Zhang, J.; Sun, J.; Maeda, K.; Domen, K.; Liu, P.; Antonietti, M.; Fu, X.; Wang, X. Sulfur-mediated synthesis of carbon nitride: band-gap engineering and improved functions for photocatalysis. *Energy & Environmental Science* **2011**, *4*, 675–678.

(10) Bhowmik, S.; Phukan, S. J.; Sah, N. K.; Roy, M.; Garai, S.; Iyer, P. K. Review of Graphitic Carbon Nitride and Its Composite Catalysts for Selective Reduction of CO2. *ACS Applied Nano Materials* **2021**, *4*, 12845–12890.

(11) Tran, D. A.; Pham, C. T. N.; Ngoc, T. N.; Phi, H. N.; Ta, Q. T. H.; Truong, D. H.; Luc, H. H.; Dao, N. N.; Kim, S. J.; Vo, V., et al. One-step synthesis of oxygen doped g-C3N4 for enhanced visible-light photodegradation of Rhodamine B. *Journal of Physics and Chemistry of Solids* **2021**, *151*, 109900.

(12) Wang, Y.; Tian, Y.; Yan, L.; Su, Z. DFT study on sulfur-doped g-C3N4 nanosheets as a photocatalyst for CO2 reduction reaction. *The Journal of Physical Chemistry C* **2018**, *122*, 7712–7719.

(13) Ding, K.; Wen, L.; Huang, M.; Zhang, Y.; Lu, Y.; Chen, Z. How does the B, F-monodoping and B/F-codoping affect the photocatalytic water-splitting performance of gC 3 N 4? *Physical Chemistry Chemical Physics* **2016**, *18*, 19217–19226.

(14) Ranjbakhsh, E.; Izadyar, M.; Nakhaeipour, A.; Habibi-Yangjeh, A. P-doped g-C3N4 as an efficient photocatalyst for CO2 conversion into value-added materials: a joint experimental and theoretical study. *International Journal of Quantum Chemistry* **2020**, *120*, e26388.

(15) Ao, C.; Feng, B.; Qian, S.; Wang, L.; Zhao, W.; Zhai, Y.; Zhang, L. Theoretical study of transition metals supported on g-C3N4 as electrochemical catalysts for CO2 reduction to CH3OH and CH4. *Journal of CO2 Utilization* **2020**, *36*, 116–123.

(16) Homlamai, K.; Maihom, T.; Choomwattana, S.; Sawangphruk, M.; Limtrakul, J. Single-atoms supported (Fe, Co, Ni, Cu) on graphitic carbon nitride for CO2 adsorption and hydrogenation to formic acid: First-principles insights. *Applied Surface Science* **2020**, *499*, 143928.

(17) Kresse, G.; Hafner, J. Ab initio molecular dynamics for liquid metals. *Physical Review B* **1993**, *47*, 558–561.

(18) Kresse, G.; Hafner, J. Ab initio molecular-dynamics simulation of the liquid-

metalamorphous- semiconductor transition in germanium. *Physical Review B* **1994**, *49*, 14251–14269.

(19) Kresse, G.; Furthmüller, J. Efficient iterative schemes for ab initio total-energy calculations using a plane-wave basis set. *Physical Review B - Condensed Matter and Materials Physics* **1996**, *54*, 11169–11186.

(20) Kresse, G.; Furthmüller, J. Efficiency of ab-initio total energy calculations for metals and semiconductors using a plane-wave basis set. *Computational Materials Science* **1996**, *6*, 15–50.

(21) Blöchl, P. E. Projector augmented-wave method. *Physical Review B* **1994**, *50*, 17953–17979.

(22) G. Kresse and D. Joubert, From ultrasoft pseudopotentials to the projector augmented-wave method. *Physical Review B - Condensed Matter and Materials Physics* **1999**, *59*, 1758–1775.

(23) Perdew, J. P.; Burke, K.; Ernzerhof, M. Generalized gradient approximation made simple. *Physical Review Letters* **1996**, *77*, 3865–3868.

(24) Perdew, J. P.; Burke, K.; Ernzerhof, M. Generalized Gradient Approximation Made Simple [Phys. Rev. Lett. 77, 3865 (1996)]. *Phys. Rev. Lett.* **1997**, *78*, 1396–1396.

(25) Heyd, J.; Scuseria, G. E.; Ernzerhof, M. Hybrid functionals based on a screened Coulomb potential. *The Journal of chemical physics* **2003**, *118*, 8207–8215.

(26) Grimme, S.; Ehrlich, S.; Goerigk, L. Effect of the damping function in dispersion corrected density functional theory. *Journal of computational chemistry* **2011**, *32*, 1456–1465.

(27) Grimme, S.; Antony, J.; Ehrlich, S.; Krieg, H. A consistent and accurate ab initio

parametrization of density functional dispersion correction (DFT-D) for the 94 elements H-Pu. *The Journal of chemical physics* **2010**, *132*, 154104.

(28) Monkhorst, H. J.; Pack, J. D. Special points for Brillouin-zone integrations. *Physical review B* **1976**, *13*, 5188.

(29) Gorai, D. K.; Kundu, T. Influence of Pt and P doping on the performance of g-C3N4 monolayer. *Materials and Manufacturing Processes* **2020**, *35*, 625–634.

(30) Wei, B.; Wang, W.; Sun, J.; Mei, Q.; An, Z.; Cao, H.; Han, D.; Xie, J.; Zhan, J.; He, M. Insight into the effect of boron doping on electronic structure, photocatalytic and adsorption performance of g-C3N4 by first-principles study. *Applied Surface Science* **2020**, *511*, 145549.

(31) Zhu, B.; Zhang, L.; Xu, D.; Cheng, B.; Yu, J. Adsorption investigation of CO2 on g-C3N4 surface by DFT calculation. *Journal of CO2 Utilization* **2017**, *21*, 327–335.

(32) Komatsu, T. Prototype carbon nitrides similar to the symmetric triangular form of melon. *Journal of Materials Chemistry* **2001**, *11*, 802–803.

(33) Bojdys, M. J.; Müller, J.-O.; Antonietti, M.; Thomas, A. Ionothermal synthesis of crystalline, condensed, graphitic carbon nitride. *Chemistry–A European Journal* **2008**, *14*, 8177–8182.

(34) Azofra, L. M.; MacFarlane, D. R.; Sun, C. A DFT study of planar vs. corrugated graphene-like carbon nitride (gC 3 N 4) and its role in the catalytic performance of CO 2 conversion. *Physical Chemistry Chemical Physics* **2016**, *18*, 18507–18514.

(35) Bhagat, B.; Dashora, A. Understanding the synergistic effect of Co-loading and B-doping in g-C3N4 for enhanced photocatalytic activity for overall solar water splitting. *Carbon* **2021**, *178*, 666–677.

(36) Yu, H.; Jiang, X.; Shao, Z.; Feng, J.; Yang, X.; Liu, Y. Metal-Free Half-Metallicity in B-Doped gh-C3N4 Systems. *Nanoscale Research Letters* **2018**, *13*.

(37) Stolbov, S.; Zuluaga, S. Sulfur doping effects on the electronic and geometric structures of graphitic carbon nitride photocatalyst: insights from first principles. *Journal of Physics: Condensed Matter* **2013**, *25*, 085507.

(38) Chen, G.; Gao, S.-P. Structure and electronic structure of S-doped graphitic C3N4 investigated by density functional theory. *Chinese Physics B* **2012**, *21*, 107101.

(39) Cui, J.; Liang, S.; Wang, X.; Zhang, J. First principle modeling of oxygen-doped monolayer graphitic carbon nitride. *Materials Chemistry and Physics* **2015**, *161*, 194–200.

(40) Huang, Z.-F.; Song, J.; Pan, L.; Wang, Z.; Zhang, X.; Zou, J.-J.; Mi, W.; Zhang, X.; Wang, L. Carbon nitride with simultaneous porous network and O-doping for efficient solar-energy-driven hydrogen evolution. *Nano Energy* **2015**, *12*, 646–656.

(41) Molaei, M.; Mousavi-Khoshdel, S. M.; Ghiasi, M. Exploring the effect of phosphorus doping on the utility of gC 3 N 4 as an electrode material in Na-ion batteries using DFT method. *Journal of Molecular Modeling* **2019**, *25*, 1–8.

(42) Zheng, Q.; Durkin, D. P.; Elenewski, J. E.; Sun, Y.; Banek, N. A.; Hua, L.; Chen, H.; Wagner, M. J.; Zhang, W.; Shuai, D. Visible-light-responsive graphitic carbon nitride: rational design and photocatalytic applications for water treatment. *Environmental science & technology* **2016**, *50*, 12938–12948.

(43) Zhang, H.-p.; Du, A.; Gandhi, N. S.; Jiao, Y.; Zhang, Y.; Lin, X.; Lu, X.; Tang, Y. Metal-doped graphitic carbon nitride (g-C3N4) as selective NO2 sensors: a first-principles study. *Applied Surface Science* **2018**, *455*, 1116–1122.

(44) Guo, C.; Zhang, T.; Deng, X.; Liang, X.; Guo, W.; Lu, X.; Wu, L. Electrochemical